Multiple-Edge XAS Studies of Synthetic Iron−Copper Bridged Molecular Assemblies Relevant to Cytochrome *c* Oxidase. Structure Determination Using Multiple-Scattering Analysis with Statistical Evaluation of Errors

Hua Holly Zhang,[†] Adriano Filipponi,[§,⊥] Andrea Di Cicco,[‡,▽] Sonny C. Lee,[∥] Michael J. Scott,[∥] R. H. Holm,*[,∥] Britt Hedman,*[,‡] and Keith O. Hodgson*[,†,‡]

Department of Chemistry, Stanford University, Stanford, California 94305, European Synchrotron Radiation Facility, B.P. 220, F-38043 Grenoble, France, Stanford Synchrotron Radiation Laboratory, Stanford University, Stanford, California 94309, and Department of Chemistry, Harvard University, Cambridge, Massachusetts 02138

Received January 10, 1996[⊗]

An X-ray absorption spectroscopy study has been carried out at the Fe and Cu K-edges for two bridged molecular assemblies, both of which contain an Fe−X−Cu (X = O^{2-}, OH^-) bridge unit, some of whose features are relevant to the binuclear site of cytochrome *c* oxidase. The two complexes $[(OEP)Fe-O-Cu(Me_6tren)]^{1+}$ and $[(OEP)-Fe-(OH)-Cu(Me_5tren)(OClO_3)]^{1+}$ have similar structural fragments around the metal centers except that they differ significantly in the bridge structure (the former contains a linear oxo bridge while the latter has a bent hydroxo bridge). We report a comparative study of these complexes using multiple-scattering (MS) EXAFS analysis and the program package GNXAS. It is found that there is a dramatic increase in the amplitude of the Fe−X−Cu MS pathway as the bridge unit approaches linearity. Full EXAFS MS analysis enables accurate quantitation of bridge metrical details and geometry for both complexes. These studies were done with an expanded version of GNXAS, which allows for simultaneous multiple-edge fitting. Such multiple-edge analysis (using both Fe and Cu edge data) allows common pathways (in this case involving the Fe−X−Cu bridge) to be constrained to be the same, thus improving the observation/variable ratio and enhancing sensitivity for determination of the bridge structure. The accuracy of the structural determination for the bridge units is evaluated by a statistical analysis methodology in which correlations among fitting parameters are identified and contour plots are used to determine random error. The overall error in the EXAFS structural determination is found by establishing the variance with the crystallographically determined values: for the EXAFS-determined parameters at distances below 4 Å, distances and angles deviated on average from crystallographic values by 0.014 Å and 1.5°, respectively. It is also established that structural features in the Fe absorption preedge are diagnostic of oxo *vs* hydroxo ligation. The relevance of this study to the structural definition of binuclear bridged sites in cytochrome *c* oxidase and other metalloenzymes is considered.

Introduction

The terminal event in eukaryotic respiration is the four-electron reduction of dioxygen to water, catalyzed by mitochondrial and bacterial oxidases which form a superfamily of heme−copper respiratory oxidases.[1−5] These enzymes are known to possess multiple metal centers: a binuclear Cu_A site,[6−8] a heme *a* center, and a binuclear heme−copper unit (heme a_3-Cu_B) which is the locus of dioxygen binding and reduction. In bacterial oxidases, the Cu_A site may be absent. In work of great significance to the oxidase problem, the structures of the enzymes from *Paracoccus denitrificans*[9] and beef heart mitochondria[10] have been crystallographically defined at 2.8 Å resolution. The array of metal centers has been confirmed, and the separations between iron and copper atoms in the binuclear site have been found to be 5.2 and 4.5 Å in the resting forms of the bacterial and mammalian enzymes, respectively. These structures do not reveal the identity of the bridging ligand(s) which modulate antiferromagnetic coupling between Fe(III) and Cu(II) affording an $S = 2$ ground state in the oxidized form of the enzymes.[11]

We have pursued the structural and electronic nature of the binuclear enzyme site by the synthesis and characterization of heme-based molecular complexes containing the bridge unit $[Fe^{III}-X-Cu^{II}]$ with X = O^{2-},[12] OH^-,[13] CN^-,[14−16] F^-,[17] and RCO_2^-.[18] The latter three bridging species are enzyme inhibitors, whereas the first two are possible bridges in the oxidized

* To whom correspondence should be addressed.
† Department of Chemistry, Stanford University.
‡ Stanford Synchrotron Radiation Laboratory, Stanford University.
§ European Synchrotron Radiation Facility.
∥ Harvard University.
⊥ Permanent address: Dipartimento di Fisica, Università degli Studi dell' Aquila, Via Vetoio, 67010 Coppito, L'Aquila, Italy.
▽ Permanent address: Dipartimento di Matematica e Fisica, Università degli Studi di Camerino, Via Madonna delle Carceri, 62032 Camerino (MC), Italy.
⊗ Abstract published in *Advance ACS Abstracts,* July 1, 1996.

(1) Babcock, G. T.; Wikström, M. *Nature* **1992**, *356*, 301.
(2) Chan, S. I.; Li, P. M. *Biochemistry* **1990**, *29*, 1.
(3) García-Horsman, J. A.; Barquera, B.; Rumbley, J.; Ma, J.; Gennis, R. B. *J. Bacteriol.* **1994**, *176*, 5587.
(4) Malmström, B. G. *Chem. Rev.* **1990**, *90*, 1247.
(5) Einarsdóttir, O. *Biochim. Biophys. Acta* **1995**, *1229*, 129.
(6) Malmström, B. G.; Aasa, R. *FEBS Lett.* **1993**, *325*, 49.
(7) Kelly, M.; Lappalainen, P.; Talbo, G.; Haltia, T.; van der Ooost, J.; Saratse, M. *J. Biol. Chem.* **1993**, *268*, 16781 .
(8) Blackburn, N. J.; Barr, M. E.; Woodruff, W. H.; van der Ooost, J.; de Vries, S. *Biochemistry* **1994**, *33*, 10401.
(9) Iwata, S.; Ostermeier, C.; Ludwig, B.; Michel, H. *Nature* **1995**, *376*, 660.
(10) Tsukihara, T.; Aoyama, H.; Yamashita, E.; Tomizaki, T.; Yamaguchi, H.; Shinzawa-Itoh, K.; Nakashima, R.; Yaono, R.; Yoshikawa, S. *Science* **1995**, *269*, 1069; **1996**, *272*, 1136.
(11) This state has been directly established for the mammalian oxidase. Day, E. P.; Peterson, J.; Sendova, M. S.; Schoonover, J.; Palmer, G. *Biochemistry* **1993**, *32*, 7855.

S0020-1669(96)00021-3 CCC: $12.00

resting enzymes. Two of the oxygen-bridged assemblies, $[(OEP)Fe-O-Cu(Me_6tren)]^{1+}$ [12] ("oxo") and $[(OEP)Fe-(OH)-Cu(Me_5tren)(OClO_3)]^{1+}$ [13] ("hydroxo") are the subjects of this investigation; for brevity, they will be referred to by the indicated simplified names. The two complexes differ significantly in the crystallographically determined Fe−O−Cu bridge angle, the oxo complex being practically linear (175.2(3)°) and the hydroxo complex being markedly bent (157.0(2)°). Karlin *et al.*[19a] have described a nearly linear oxo-bridged species and demonstrated its protonation to a bridged hydroxo species, whose X-ray crystal structure has thus far not been reported.[19b] Consequently, the preceding oxo/hydroxo pair forms a unique set of structurally defined bridged assemblies with which to examine the effect of bridge angle at constant bridge atom on Cu and Fe extended X-ray absorption fine structure (EXAFS). X-ray crystal structures of the complexes[12,13] are represented in Figure 1, and selected metric data are collected in Tables 1 and 2.

The oxo and hydroxo complexes present a significant challenge for multiple-scattering (MS) EXAFS analysis. In the Fe EXAFS, the rigid porphyrin ligand contributes strong MS terms to the total EXAFS signal.[13] Furthermore, MS effects are expected to become especially significant for a monoatomic bridge which approaches linearity. A focusing effect occurs when the intervening atom is placed linearly between the photoabsorber and the backscatterer, resulting in a significant amplitude enhancement in the EXAFS signal.[20,21] We have undertaken EXAFS analyses of these complexes in an effort to develop further the MS EXAFS methodology, such that bridge angles and distances can be determined in cases where X-ray structural definition is lacking. An ultimate goal is the application of this methodology to the binuclear sites of oxidases in various reaction states—resting, catalytic, inhibitory—of the enzymes. In the full study reported here, we have measured high-quality EXAFS data for the oxo and hydroxo complexes at both the Fe and Cu K-edges to provide complementary information about the bridges. The Fe EXAFS data analysis allows the study of MS pathways which include the porphyrin framework. Because porphyrin MS contributions occur in the same region as the Fe−O−Cu bridge signal, the impact of porphyrin MS effects on structure determination of the bridge can be evaluated. From the Cu K-edge, more reliable bridge parameters may be anticipated in the absence of porphyrin MS effects.

The data were analyzed using an expanded version of the integrated EXAFS package GNXAS, which is based on full curved wave, MS theoretical analysis.[22,23] GNXAS incorporates direct fitting of theoretical signals to the experimental data using the Hedin−Lundqvist complex exchange and correlation potentials. In addition to single-scattering (SS) signals, GNXAS accounts for MS paths with correct treatment of the configurational average of all MS signals to allow fitting of correlated distances and bond variances σ_R^2 (Debye−Waller-like factors). Therefore, GNXAS is particularly well-suited for MS analysis and angle determination. A quantitative examination of MS effects on Fe−nitrosyl complexes utilizing GNXAS has shown that the MS analysis is very sensitive to angles between 150 and 180°.[24] We have also demonstrated that GNXAS is able to evaluate long-range interactions to *ca.* 5.0 Å using MS signals, thereby providing reliable angle and distance information for second- and third-shell scatterers in synthetic[25] and native[26] metal clusters.

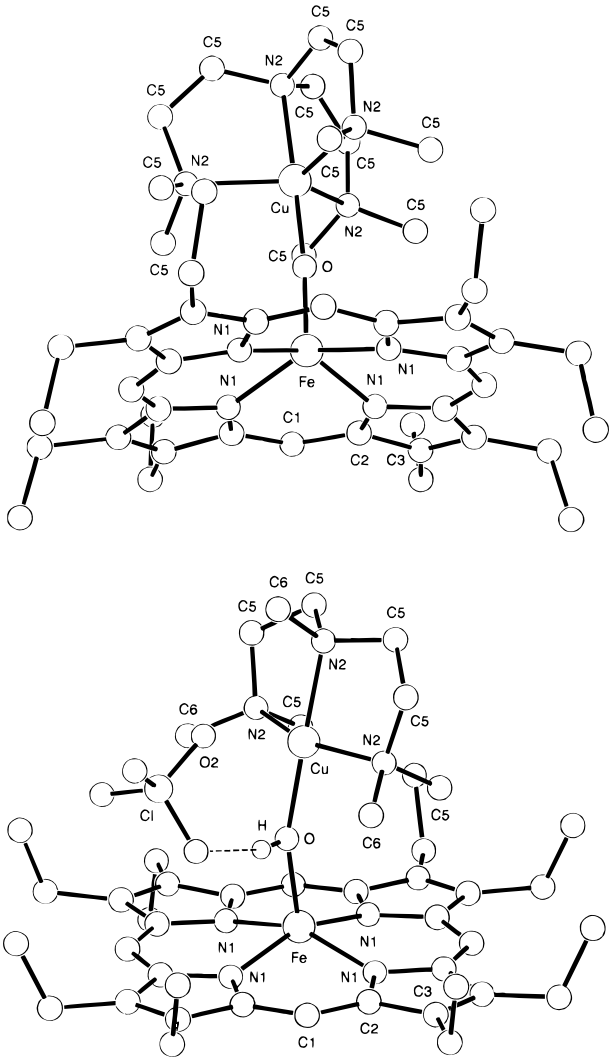

Figure 1. Molecular structures of $[(OEP)Fe-O-Cu(Me_6tren)]^{1+}$ (oxo, top) and $[(OEP)Fe-(OH)-Cu(Me_5dien)(OClO_3)]^{1+}$ (hydroxo, bottom) complexes. Notable is the linear (oxo) *vs* bent (hydroxo) bridge which significantly influences the EXAFS signal of this unit.

(12) Lee, S. C.; Holm, R. H. *J. Am. Chem. Soc.* **1993**, *115*, 5833,11789. OEP = octaethylporphyrinate(1−); Me_6tren = tris(2-(dimethylamino)-ethyl)amine.
(13) Scott, M. J.; Zhang, H. H.; Lee, S. C.; Hedman, B.; Hodgson, K. O.; Holm, R. H. *J. Am. Chem. Soc.* **1995**, *117*, 568. Me_5tren = 1,1,4,7,7-pentamethyldiethylenetriamine.
(14) Scott, M. J.; Lee, S. C.; Holm, R. H. *Inorg. Chem.* **1994**, *33*, 4651.
(15) Scott, M. J.; Holm, R. H. *J. Am. Chem. Soc.* **1994**, *116*, 11357.
(16) Lee, S. C.; Scott, M. J.; Kauffmann, K.; Münck, E.; Holm, R. H. *J. Am. Chem. Soc.* **1994**, *116*, 401.
(17) Lee, S. C.; Holm, R. H. *Inorg. Chem.* **1993**, *32*, 4745.
(18) Scott, M. J.; Goddard, C. A.; Holm, R. H. *Inorg. Chem.* **1996**, *35*, 2558.
(19) (a) Karlin, K. D.; Nanthakumar, A.; Fox, S.; Murthy, N. N.; Ravi, N.; Huynh, B. H.; Orosz, R. D.; Day, E. P. *J. Am. Chem. Soc.* **1994**, *116*, 4753. (b) After this manuscript was submitted for publication, Karlin and co-workers reported the EXAFS analysis of a $Fe^{III}-(OH)-Cu^{II}$ complex with $\angle Fe-O(H)-Cu = 157 \pm 5°$: Fox, S.; Nanthakumar, A.; Wikström, M.; Karlin, K. D.; Blackburn, N. J. *J. Am. Chem. Soc.* **1996**, *118*, 24.
(20) Teo, B. K. *J. Am. Chem. Soc.* **1981**, *103*, 3990.
(21) Co, M. S.; Hendrickson, W. A.; Hodgson, K. O.; Doniach, S. *J. Am. Chem. Soc.* **1983**, *105*, 1144.
(22) Filipponi, A.; Di Cicco, A.; Natoli, C. R. *Phys. Rev. B* **1995**, *52*, 15122.
(23) Filipponi, A.; Di Cicco, A. *Phys. Rev. B* **1995**, *52*, 15135.
(24) Westre, T. E.; Di Cicco, A.; Filipponi, A.; Natoli, C. R.; Hedman, B.; Solomon, E. I.; Hodgson, K. O. *J. Am. Chem. Soc.* **1994**, *116*, 6757.
(25) Nordlander, E.; Lee, S. C.; Cen, W.; Wu, Z. Y.; Filipponi, A.; Di Cicco, A.; Natoli, C. R.; Hedman, B.; Hodgson, K. O.; Holm, R. H. *J. Am. Chem. Soc.* **1993**, *115*, 5549.
(26) Liu, H. I.; Filipponi, A.; Gavini, N.; Burgess, B. K.; Hedman, B.; Di Cicco, A.; Natoli, C. R.; Hodgson, K. O. *J. Am. Chem. Soc.* **1994**, *116*, 2418.

Table 1. Comparison of Selected GNXAS Fit Results with Crystallographic Values for the $Fe^{III}-O-Cu^{II}$ Bridge of $[(OEP)Fe-O-Cu(Me_6tren)]^{1+}$

structural feature	crystallographic average value (range)[a]	Fe single K-edge distance/angle (bond/angle variance)[b]	Cu single K-edge distance/angle (bond/angle variance)[b]	Fe + Cu multiple K-edge distance/angle (bond/angle variance)[b]
Cu−O	1.83 Å	1.83 Å (0.001)	1.84 Å (0.001)	1.84 Å (0.001)
Cu−N2	2.11 (2.05−2.15) Å		2.14 Å (0.008)	2.14 Å (0.007)
Cu−C5	2.93 (2.80−3.03) Å		2.96 Å (0.007)	2.95 Å (0.007)
Fe−O	1.75 Å	1.75 Å (0.003)	1.75 Å (0.004)	1.74 Å (0.002)
Fe−N1	2.11 (2.10−2.12) Å	2.10 Å (0.002)		2.10 Å (0.002)
Fe−C2	3.12 (3.09−3.13) Å	3.13 Å (0.004)		3.12 Å (0.004)
Fe−C1	3.48 (3.47−3.49) Å	3.47 Å (0.001)		3.47 Å (0.001)
Fe−C3	4.35 (4.32−4.37) Å	4.39 Å (0.004)		4.41 Å (0.007)
Fe−N/C	4.36 (4.30−4.38) Å	4.24 Å (0.007)		
Fe−Cu	3.57 Å	3.58 Å (0.003)	3.57 Å (0.002)	3.58 Å (0.002)
Fe−O−Cu	175.3°	180° (9×10^0)	180° (4×10^0)	180° (3×10^1)
Cu−N2−C5	108.5° (105.8−114.2°)		107° (6×10^1)	108° (1×10^1)
Fe−N1−C2	126.2° (124.4−127.1°)	126° (3×10^1)		126° (1×10^1)
Fe−N1−C3	159.5° (157.2−161.4°)	159° (5×10^0)		159° (1×10^1)

[a] Reference 12. [b] Bond and angle variances are reported in $Å^2$ and deg^2, respectively.

Table 2. Comparison of Selected GNXAS Fit Results with Crystallographic Values for the $Fe^{III}-O(H)-Cu^{II}$ Bridge of $[(OEP)Fe-(OH)-Cu(Me_5dien)](OClO_3)]^{1+}$

structural feature	crystallographic average value (range)[a]	Fe single K-edge distance/angle (bond/angle variance)[b]	Cu single K-edge distance/angle (bond/angle variance)[b]	Fe + Cu multiple K-edge distance/angle (bond/angle variance)[b]
Cu−O(H)	1.95 Å	1.98 Å (0.005)	1.96 Å (0.005)	1.99 Å (0.001)
Cu−N2	2.03 (2.02−2.04) Å		2.04 Å (0.003)	2.04 Å (0.005)
Cu−O2	2.43 Å		2.42 Å (0.006)	2.40 Å (0.004)
Cu−C5	2.82 (2.81−2.85) Å		2.85 Å (0.002)	2.86 Å (0.002)
Cu−C6	2.97 (2.97−2.98) Å		2.98 Å (0.002)	3.00 Å (0.002)
Cu−Cl	3.54 Å		3.54 Å (0.003)	3.52 Å (0.006)
Cu−O3	3.57 Å		3.58 Å (0.004)	
Fe−O(H)	1.93 Å	1.91 Å (0.006)	1.92 Å (0.001)	1.93 Å (0.003)
Fe−N1	2.04 (2.04−2.05) Å	2.04 Å (0.002)		2.05 Å (0.002)
Fe−C2	3.07 (3.04−3.09) Å	3.09 Å (0.004)		3.09 Å (0.003)
Fe−C1	3.42 (3.39−3.44) Å	3.42 Å (0.005)		3.41 Å (0.005)
Fe−C3	4.28 (4.26−4.29) Å	4.36 Å (0.005)		4.35 Å (0.003)
Fe−N/C	4.36 (4.32−4.39) Å	4.33 Å (0.01)		
Fe−Cu	3.80 Å	3.78 Å (0.005)	3.82 Å (0.006)	3.81 Å (0.003)
Fe−O(H)−Cu	157.0°	154° (2×10^1)	161° (7×10^0)	154° (6×10^1)
Cu−N2−C5	106.2° (104.8−107.6°)		105° (6×10^0)	107° (7×10^0)
Cu−N2−C6	115.1° (114.6−115.6°)		113° (3×10^0)	115° (2×10^1)
Cu−O2−Cl	131.6°		132° (6×10^0)	137° (7×10^0)
Fe−N1−C2	126.6° (125.1−127.6°)	126° (7×10^0)		123° (6×10^0)
Fe−N1−C3	159.9° (157.8−161.5°)	161° (7×10^0)		159° (7×10^0)

[a] Reference 13. [b] Bond and angle variances are reported in $Å^2$ and deg^2, respectively.

Earlier, we have described preliminary Fe K-edge data analysis of the oxo and hydroxo complexes.[13] We have completed our analysis of both Fe and Cu K-edge EXAFS data for the two complexes and report the full set of results and conclusions here. In this context, we note certain recent EXAFS results on a bacterial oxidase[27,28] and on a mitochondria oxidase[29] and consider those findings in relation to the properties of the synthetic bridged assemblies. Further, we describe the utilization, for the first time with GNXAS, of simultaneous least-squares fitting[30] of an entire molecular complex *vs* Fe *and* Cu K-edge data, in which common structural units share a subset of parameters. This approach offers a possible enhancement of the sensitivity to the determination of the Fe−X−Cu bridge and is compared to results obtained from refinements *vs* the individual data sets. Finally, we apply a statistical analysis methodology that allows a more rigorous evaluation of statistical errors in the fits in parameter space.[23,31] The approach provides information on statistical correlation among fitting parameters and thereby identifies parameters which can be measured reliably and those which are underdetermined.

Experimental Section

Sample Preparation and Data Collection and Reduction. X-ray absorption spectroscopy (XAS) powder samples of the oxo[12] and hydroxo[13] complexes were prepared in an inert atmosphere, nitrogen-filled, dry glovebox. The samples were mixed with boron nitride and ground into a fine powder. Each was transferred into a 1 mm thick slotted Al spacer, pressed into a fine pellet, and sealed between 63.5 μm Mylar windows. Upon removal from the glovebox, the samples were immediately frozen in liquid nitrogen and kept at this temperature prior to the measurements.

X-ray absorption spectroscopic data at the Fe and Cu K-edges were recorded at the Stanford Synchrotron Radiation Laboratory (SSRL) on

(27) Powers, L.; Lauraeus, M.; Reddy, K. S.; Chance, B.; Wikström, M. *Biochim. Biophys. Acta* **1994**, *1183*, 504.
(28) Fann, Y. C.; Ahmed, I.; Blackburn, N. J.; Boswell, J. S.; Verkhovskaya, M. L.; Hoffman, B. M.; Wikström, M. *Biochemistry* **1995**, *34*, 10245.
(29) Henkel, G.; Müller, A.; Weissgräber, S.; Buse, G.; Soulimane, T.; Steffens, G. C. M.; Nolting, J.-F. *Angew. Chem., Int. Ed. Engl.* **1995**, *34*, 1488.
(30) Di Cicco, A. *Phys. Rev. B* **1996**, *53*, 6174.
(31) Filipponi, A. *J. Phys.: Condens. Matter* **1995**, *7*, 9343.

unfocused beamline 7−3 with ring conditions 3.0 GeV and 60−100 mA. A Si(220) double-crystal monochromator was used, and the vertical beam aperture was defined to be 1 mm before the monochromator. Transmission data were measured with three nitrogen-filled ionization chambers, with a Fe or Cu foil placed between the second and the third ionization chambers for internal calibration. The measurements were performed at a constant temperature of 10 K, maintained by an Oxford Instruments CF1208 continuous flow, liquid helium cryostat.

During data reduction, energy calibration was performed using the internal foil spectra and assigning the first inflection points to be 7111.2 eV (Fe) and 8980.3 eV (Cu). The data represent an average of four to five scans, with data reduction according to previously published methods.[32,33]

GNXAS Data Analysis. The theoretical basis for the GNXAS approach and its fitting methodologies have been described in detail elsewhere.[22,23,34] For the study reported herein, the crystallographic coordinates for the oxo[12] and the hydroxo[13] complexes were used as input to generate an initial structural model up to a distance cutoff of 4.5 Å. Phase shifts were calculated using the standard muffin-tin approximation up to an energy limit of 70 Ry (952 eV) above the Fe and Cu K-edges, which were then used to calculate individual two-body and three-body EXAFS signals according to criteria described previously.[34] The least-squares minimization program which uses the MINUIT subroutine of the CERN library was used in direct fitting of the averaged raw absorption data with a model EXAFS spectrum. This model spectrum consists of a calculated total EXAFS signal, double-electron excitation contributions, and an appropriate background. The background was modeled as a polynomial for the preedge and as a series of smooth polynomial splines of specific orders accounting for the postedge background effects which were refined during the fitting procedure by varying the coefficients of the polynomials to minimize the difference between the theoretical and experimental signals. The structural parameters varied during the refinements were the bond distance (R) and the bond variance (σ^2_R) for a two-body signal, the two bond distances (R_1 and R_2), the angle (θ) between the two bonds, and the six covariance matrix elements: bond variances ($\sigma^2_{R_1}$ and $\sigma^2_{R_2}$), angle variance (δ^2_θ for an angle of 180°; σ^2_θ for an angle <180°),[23] bond−bond correlation (ρ_{R_1,R_2}), and bond−angle correlations ($\rho_{R_1,\theta}$ and $\rho_{R_2,\theta}$) for a three-body signal. The thermal vibration and the static disorder were accounted for by the value of σ^2_R for a two-body configuration and by the values of the six covariance matrix elements for a three-body configuration. The coordination numbers were fixed at the known crystallographic values. The nonstructural parameters varied were E_0, S_0^2 (many-body amplitude reduction factor), Γ_e (effective mean-free path parameter), and E_r (experimental resolution). All parameters were allowed to vary within a preset range, and the results were checked to ensure that the refined values did not reach the upper- or the lower-range boundary.

During the refinement, individual signals for two-body and three-body contributions were systematically included in the fit. The first-shell two-body signals were optimized by comparing the corresponding theoretical and experimental Fourier transform (FT) peaks. The outer-shell two-body and three-body contributions were then added. Strong three-body MS signals were identified by examining the magnitude of the calculated model signals of the various configurations and were usually those with a bond angle greater than 150° and/or with a bond multiplicity >3. The second-shell $\gamma^{(2)}$ signal associated with the most distant atom (when present) and the three-body MS $\gamma^{(3)}$ signal were combined to form a total effective signal related to a particular three-body configuration.[22] The quality of the fit was monitored by the goodness-of-fit value *R* (for definition, see ref 34) and by the agreement of the refined theoretical EXAFS signal with the experimental data as well as the residual and its FT. The final spline was in two segments of order 4,4 in the energy intervals between 7200, 7500, and 7980 eV and 9040, 9260, and 9650 eV for Fe and Cu data, respectively. The first energy point included in the fit was chosen to minimize the level of the residual FT spectrum for R < 1.0 Å. The optimal parameters obtained from these Fe and Cu single-edge fits were then combined and served as initial values in the multiple-edge fitting procedure, in which one model based on theoretical signals calculated from the individual edges was refined simultaneously *vs* the Fe and Cu K-edge data sets.

The calculation of a nearly linear three-body signal can be approached in two ways in GNXAS.[35] The presented results for the oxo case represent fits with a fixed 180° Fe−O−Cu bond angle. With these fits, $\rho_{R_1,\theta}$ and $\rho_{R_2,\theta}$ must be zero because of odd parity in θ. Therefore, for the three-body Fe−O−Cu bridge configuration, only the nonzero covariance matrix elements $\sigma^2_{R_1}$, $\sigma^2_{R_2}$, δ^2_θ, and ρ_{R_1,R_2} were varied.

As discussed elsewhere,[34,36] a comparison between the number of independent points in the EXAFS spectrum with the number of independent variables in a given fit is helpful in indicating if the nonlinear least-squares procedure is likely to be well-determined and not lead to parameters with very large errors. For the final fits discussed later, the ratio of the total number of parameters N_{par} and the number of independent points N_{ind} (estimated according to Stern[36]) (N_{par}/N_{ind}) was the following: oxo Fe K-edge (30/32); oxo Cu K-edge (19/29); hydroxo Fe K-edge (33/32); hydroxo Cu K-edge (38/29); multiple-edge oxo (40/61); multiple-edge hydroxo (48/62). For all these cases except the hydroxo Cu K-edge fits, the ratio indicates that the number of variables in the fit is justified. For the hydroxo Cu K-edge fit, high errors on individual fit parameters would be indicative of problems with the determination of those values.

After a good minimum was obtained, a procedure for evaluating the statistical significance of the variables associated with the bridge structure followed. With all other parameters fixed at the values for the best fit minimum, another minimization routine was performed on the parameters of interest and the correlation coefficients between the pair of the parameters were generated. The statistical correlation was then visualized by plotting several two-dimensional intersections of the error confidence interval in parameter space, referred to as contour plots in the following discussion.

The theory of the error determination in GNXAS is described in detail elsewhere.[23,31] Briefly, the error evaluation procedure is only meaningful after all of the individual signals contributing to the total EXAFS are well accounted for. At this level of refinement, the residual function *R* must be dominated only by random noise and is described by a χ^2_{N-p} distribution with $N - p$ degrees of freedom, where *N* is the number of experimental data points and *p* is the number of fitting variables, namely $R = \chi^2_{N-p}$.

The confidence intervals in the *p* parameter space are defined as the region enclosed by the $(p - 1)$-dimensional surface defined by the following equation

$$R = R_{min} + C \tag{1}$$

where R_{min} is the minimum of the residual function *R* and *C* is the critical value for the χ^2_p random variable corresponding to the 95% confidence interval. It is important to remark that *C* depends on the actual number of parameters *p*. For $p > 2$, the actual shape of the confidence intervals can be inferred from many two-dimensional contour plots representing the intersection between the true surface and the selected two-parameter plane. The two-dimensional contour plots have approximately ellipsoidal shapes.

The contour plot gives an indication of the correlation between the selected parameters. For a parabolic minimum, the principal axis of

(32) Scott, R. A. *Methods Enzymol.* **1985**, *117*, 414.
(33) Cramer, S. P.; Hodgson, K. O. *Prog. Inorg. Chem.* **1979**, *15*, 1.
(34) Westre, T. E.; Di Cicco, A.; Filipponi, A.; Natoli, C. R.; Hedman, B.; Solomon, E. I.; Hodgson, K. O. *J. Am. Chem. Soc.* **1995**, *117*, 1566.

(35) For a three-body signal, the GNXAS program uses a first-order Taylor expansion of the amplitude and phase to calculate the configurational average of the signal. In the case of a linear structure ($\theta = 180°$), the first-order derivative vanishes and therefore second-order derivatives are used. In the nearly linear oxo bridge, the effect of thermal vibrations was modeled either as a Gaussian distribution around a slightly bent average configuration or as a vibrating collinear configuration. In the latter case, the average deviation from 180° is measured by the angle variance, as described in ref 23. Fits which varied the Fe−O−Cu angle around 175.3° (with the upper limit to be 178°) as well as fits which included a fixed angle of 180° were carried out. The two methods were found to give fits of similar quality and results, indicating that GNXAS is quite reliable in fitting linear structures.

(36) Stern, E. A. *Phys. Rev. B* **1993**, *48*, 9825.

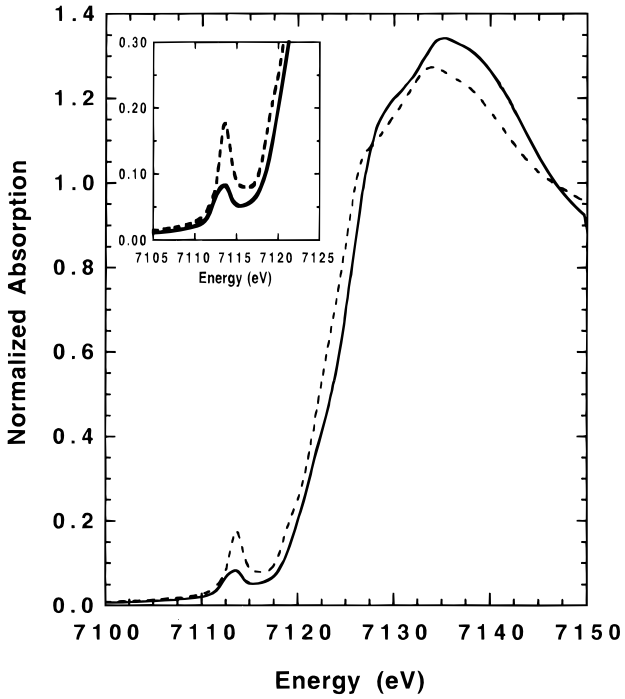

Figure 2. Normalized Fe K-edge spectra of the oxo (---) and hydroxo (—) complexes. Inset: an expansion of the 1s → 3d preedge transition region. The difference in intensity of the preedge transition is a distinguishing feature for the oxo *vs* the hydroxo bonding configuration (see text for discussion).

the ellipses is tilted proportionally to the statistical correlation among the parameters. The contour plots reported here were generated from the multiple-edge fits. The inner contour refers to the 95% error confidence interval, and the others are traced substituting n^2C (with n = 2, 3, 4, ...) for C in eq 1.

Results and Discussion

Edges. Oxo and Hydroxo Complexes. The edge regions of the XAS spectra of the two complexes were first examined. Both show preedge features at ∼7113.5 eV (Fe) and ∼8979.5 eV (Cu). The Fe K-edge spectrum is shown in Figure 2. Preedge features for first-row transition metals can provide information about the electronic and geometric structure of the metal site as they derive from a 1s → 3d transition.[37] Formally, the 1s → 3d transition is electric-dipole forbidden, but it gains intensity through an allowed quadrupole transition,[38] which is only ∼1% as intense as an allowed dipole transition.[39] However, when the metal site is in a noncentrosymmetric environment, this transition gains additional intensity through a dipole mechanism from 4p mixing into the 3d orbitals. For Fe(III), the total intensity of this preedge feature has been shown to increase with decreasing coordination number.[40]

For the Cu edges, the 1s → 3d transition is relatively weak for both complexes (not shown), rather typical for $3d^9$ systems.[41] While there are small differences in the intensity of the 1s → 3d and 1s → 4p transitions, the edge features are not distinctively diagnostic for the oxo *vs* hydroxo bridge. In contrast, the differences seen at the Fe K-edge are quite dramatic (Figure 2).

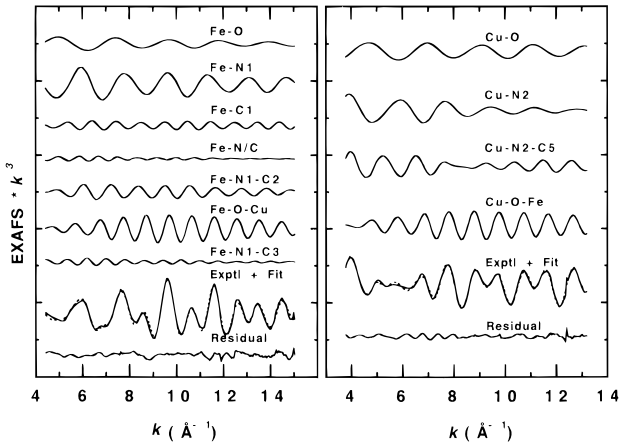

Figure 3. Individual EXAFS contributions and the total EXAFS signal (•••) compared with the experimental EXAFS data (—) for the oxo complex. Left: Fe K-edge. Right: Cu K-edge. The strong EXAFS signal from the three-body Fe−O−Cu pathway is particularly evident from both the Fe and Cu viewpoints. In both cases, the low residual is indicative of an excellent overall fit. (The ordinate scale is 10 between two consecutive tick marks.)

The iron sites of the two complexes have a square pyramidal geometry. The C_{4v} symmetry allows the 1s → 3d transition to gain intensity from both of the two intensity mechanisms described above, and therefore, the preedge features in the edge spectra of the two complexes are relatively strong. The 1s → 3d transition for the oxo complex is, however, much more intense than that for the hydroxo complex. Inspection of the metrical information about the iron site from Tables 1 and 2 reveals that the Fe−O distance of the oxo complex is ∼0.2 Å shorter than the corresponding Fe−O distance in the hydroxo complex, while the average Fe−N distance in the porphyrin is 0.07 Å longer in the oxo complex. As a result, there is more distortion in the square pyramidal geometry and the axial O ligand of the bridge is closer to the Fe site in the oxo case. This shortening of the axial bond (Fe−O) significantly alters the inversion pseudosymmetry at the Fe site, allowing more 4p mixing into the 3d orbitals, thus giving rise to a preedge feature of much higher intensity for the oxo complex.[42] Such an intensity effect has also been observed for μ-oxo bridged diiron complexes.[43] Thus, in circumstances with μ-oxo and μ-hydroxo coordination at parity of the remaining ligand set, intensity of the 1s → 3d transition can be quite diagnostic.

EXAFS. Single-Edge Fitting. The EXAFS contributions from the individual signals, the total signal compared with the experimental data for the best fit, and the residual are presented for the oxo and hydroxo complexes in Figures 3 and 4, respectively. The FTs of the experimental data sets, of the best fits, and of the residuals for all four data sets are shown in Figure

(37) Shulman, R. G.; Yafet, Y.; Eisenberger, P.; Blumberg, W. E. *Proc. Natl. Acad. Sci. U.S.A.* **1976**, *73*, 1384.
(38) Hahn, J. E.; Scott, R. A.; Hodgson, K. O.; Doniach, S.; Desjardins, S. R.; Solomon, E. I. *J. Am. Chem. Soc.* **1982**, *104*, 5364.
(39) Brouder, C. J. *J. Phys.: Condens. Matter* **1990**, *2*, 701.
(40) Roe, A. L.; Schneider, D. J.; Mayer, R. J.; Pyrz, J. W.; Widom, J.; Que, L., Jr. *J. Am. Chem. Soc.* **1984**, *106*, 1676.
(41) Shadle, S. E.; Penner-Hahn, J. E.; Schugar, H. J.; Hedman, B.; Hodgson, K. O.; Solomon, E. I. *J. Am. Chem. Soc.* **1993**, *115*, 767.
(42) The nature of the transitions for ferric iron can be understood more quantitatively. There are four many-electron excited states allowed for a high-spin ferric atom in a C_{4v} site ($^5B_2$, ^5E, $^5A_1$, and $^5B_1$). Transitions into each of these states will have quadrupole intensity. The $^5A_1$ state will have additional dipole intensity due to $4p_z$ mixing into the $3d_{z^2}$ orbital. The amount of $4p_z$ mixing into the $3d_{z^2}$ orbital will increase with a more distorted iron site (*i.e*, a shorter axial ligand) causing the transition into the $^5A_1$ state to be more intense. Thus the 1s → 3d preedge feature of the oxo-bridged complex will be more intense than that of the hydroxo-bridged complex due to the shorter Fe−O bond distance/more distorted site. The methodology describing the allowed many-electron excited states and the distribution of quadrupole and dipole intensity over those states is described in much more detail for high-spin and low-spin ferrous and ferric complexes in the following: Westre, T. E.; Kennepohl, P.; DeWitt, J. G.; Hedman, B.; Hodgson, K. O.; Solomon, E. I. *J. Am. Chem. Soc.*, to be submitted for publication.
(43) DeWitt, J. G. Ph.D. Thesis, Stanford University, CA, 1994.

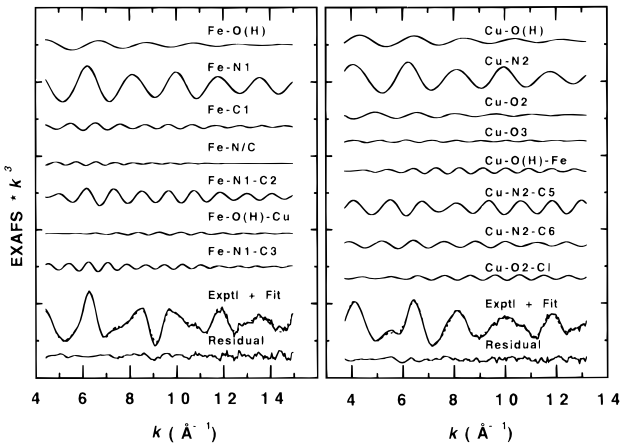

Figure 4. Individual EXAFS contributions and the total EXAFS signal (•••) compared with the experimental EXAFS data (—) for the hydroxo complex. Left: Fe K-edge. Right: Cu K-edge. The three-body Fe−O−Cu signal is relatively weak compared with the corresponding signal for the oxo complex, as shown in Figure 3. (The ordinate scale is 10 between two consecutive tick marks.)

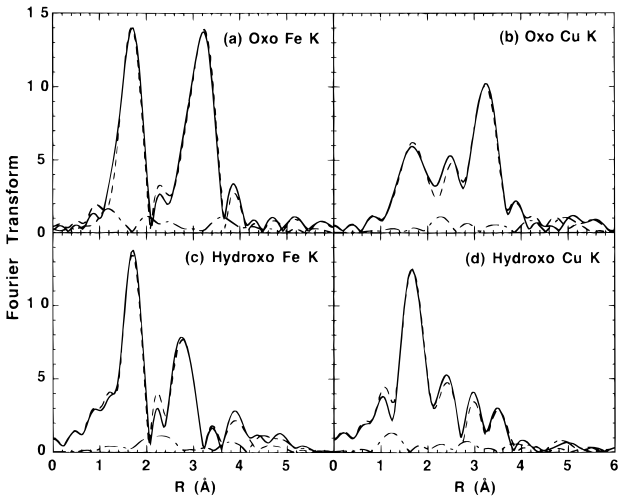

Figure 5. Comparison of non-phase-shift-corrected FTs of the experimental data (—) with those of the refined theoretical signal (---) for (a) oxo Fe K-edge, (b) oxo Cu K-edge, (c) hydroxo Fe K-edge, and (d) hydroxo Cu K-edge. Also shown are the FTs of the residuals (-•-•-). The unusually high FT peak at ∼3.1 Å for the oxo complex at both edges derives from the strong MS effect of the nearly linear Fe−O−Cu bridge. In contrast, the corresponding FT feature at ∼3.4 Å for the hydroxo complex is much smaller, reflecting the weaker MS contribution from the bent structure. Quantitation of these effects from GNXAS fits is discussed in the text.

5. Particularly striking in the FTs of the oxo compound is the unusually large feature at ∼3.1 Å (Figures 5a and 5b). This feature might be expected to result from a strong contribution from the Fe−O−Cu linear MS pathway.[34] In contrast, the FTs of the hydroxo compound have the more normal appearance one observes from the falloff in amplitude with increasing R. Overall, the fitted EXAFS spectra and their FTs match the experimental data quite well. This is also reflected in the low residuals (Figures 3 and 4) and the relatively featureless FTs of the residual (Figure 5). Selected numerical results from the fits are summarized in Tables 1 and 2.

(a) Oxo Fe K-Edge. In the fits, the lower R peak in the FT (∼1.7 Å, Figure 5a) was well accounted for by frequency contributions from two single-scattering signals, Fe−O and Fe−N1. The experimentally determined distances for the two signals show excellent agreement with the crystallographic values, deviating by <0.01 Å.

Two MS signals, Fe−O−Cu and Fe−N1−C2, along with one SS signal, Fe−Cl, mainly contribute to the FT peak at ∼3.1 Å (Figure 5a). Its main component is the Fe−O−Cu signal, whose strength is due to the strong backscattering of Cu in the linear pathway. The magnitude of this Cu backscattering signal is of the same order as that of the four two-body contributions from the Fe−N of the porphyrin (Figure 3). The signal from the multiple Fe−N1−C2 pathways is also strong, being approximately the same magnitude as for the Fe−C1 pathways. While the average Fe−N1−C2 angle is 126.2° (below the typical range where MS contribution is especially strong), the rigid porphyrin ring includes eight such three-body pathways, therefore producing a total three-body Fe−N1−C2 signal that contributes significantly. Given the large magnitude of these signals, the structural parameters obtained in the refinement of these pathways were all determined to the same distance accuracy level as for the first shell, *i.e.*, within 0.01 Å from the crystallographic values. The average fluctuation of the Fe−O−Cu bridge angle around collinearity was determined to be $\delta_\theta^2 = 9 \times 10^0$ deg^2. This means that the maximum of the bond angle probability distribution is at $\theta_{max} = 177°$. The Fe−N1−C2 angle deviated by <1° from the crystallographic value.

Two more signals were included in the fit: the three-body Fe−N1−C3, and the two-body Fe−N/C (C and N from the Me_6-tren ligand of Cu). Together they account for the FT peak at ∼3.8 Å. As would be expected, the contribution from the outer shell is small compared to the first and the second shells. The three-body Fe−N1−C3 signal is nevertheless relatively large, considering the long distance, since the average value of its angle is 159.5° and there are eight such pathways in the porphyrin ring. The structural parameters were not as accurately determined as for the first two shells. The Fe−C3 distance was found to be 0.04 Å longer than the crystallographic value. Since the three-body Fe−N1−C3 signal is in the same distance range as the two-body Fe−N/C signal, they are not resolvable given the resolution of the data, and are strongly correlated.

(b) Oxo Cu K-Edge. From a MS point of view, the Cu fragment of the oxo complex is less complicated than the Fe part, since the coordination is less regular and less rigid than for the porphyrin. In the fits, the two-body and three-body signals Cu−O, Cu−N2, Cu−N2−C5, and Cu−O−Fe were included (Figure 3). All signals were relatively strong. The linear three-body contribution from Cu−O−Fe explains the FT peak at ∼3.1 Å (Figure 5b) well, and its strong signal allowed an accurate determination of the structural parameters. The Cu−Fe distance was determined to be 3.57 Å identical to the crystallographic distance.[12] The calculated first-shell Cu−O distance was 1.84 Å. Over the large number of fits varying different structural and nonstructural parameters, the distance determination for Cu−O and Cu−Fe was remarkably consistent, with the largest deviation being <0.01 Å. The fluctuation in the Cu−O−Fe bridge angle around 180° was determined to be $\delta_\theta^2 = 4 \times 10^1$ deg^2, giving 174° as the maximum of the angle distribution which is close to the crystallographic value of 175.3°.

Structural parameters for the two-body Cu−N2 and three-body Cu−N2−C5 signals, however, showed a slightly lower degree of accuracy when compared to the crystallographic values, despite the fact that they have relatively strong signals (Figure 3). Inspection of the crystallographic results shows that there is a large spread in the four Cu−N2 distances (2.05−2.15 Å) and in the associated 12 Cu−N2−C5 angles (105.8−114.2°).[12] As a result, the long Cu−C5 separations associated with the three-body Cu−N2−C5 signal have a relatively large static disorder contribution. The best fit reflects this structural

disorder by giving a high bond variance of 0.008 and 0.007 Å^2 for the Cu−N2 and Cu−C5 distances, respectively, and an angle variance of 6×10^1 deg^2 for the Cu−N2−C5 angle. The FT peak between 2.1 and 2.8 Å is therefore less well fit (Figure 5b). Attempts to separate the Cu−N2 contribution into two shells, axial at 2.05 Å and equatorial at 2.13 Å, and consequently two three-body Cu−N2−C5 signals resulted in an increase in the *R* value and unreasonable physical parameters in some cases. Furthermore, the resulting structural parameters had large deviations from the crystallographic values with the two signals strongly correlated with each other, which would be expected since two waves at $\Delta R = 0.08$ Å are not resolvable within the Δk range of the data.

The residual of the total EXAFS signal showed some high-frequency components in the lower *k* region. This could be attributed to signals that are outside the cutoff distance of 4.5 Å and hence are not accounted for.

(c) Hydroxo Fe K-Edge. The porphyrin part of the hydroxo complex is structurally very similar to that of the oxo complex, with the Fe−N1 distance being somewhat shorter in the hydroxo case. The final fit to the data included the analogous four two-body and three three-body contributions to the total EXAFS (Figure 4).

As with the oxo complex, the first-shell contributions derive from Fe−O(H) and Fe−N1 SS signals which give rise to the FT peak at ∼1.7 Å (Figure 5c). The second FT peak at ∼2.8 Å is accounted for by the SS Fe−C1 and MS Fe−N1−C2 contributions from the porphyrin. The signal from the Fe−O(H)−Cu MS pathway is very small and contributes mainly in the small FT peak at ∼3.4 Å. The region is, however, poorly fit if this contribution is omitted, and the *R* value decreased by ∼25% upon the inclusion of the signal. The interaction of Fe with the Cu fragment (equatorial N and methyl C) results in the SS signal Fe−N/C, which, along with the MS Fe−N1−C3 signal of the porphyrin, contributes to the FT peak in the ∼3.9 Å region. As can be seen from Figure 4, among the three MS contributions, the dominant signal is the three-body Fe−N1−C2 pathway from the porphyrin. This is in sharp contrast with the oxo case where the linear Fe−O−Cu signal was the strongest.

The fitted theoretical signal matched the experimental data (Figure 5c) quite well, and the structural parameters obtained from GNXAS were all within 2% of the crystallographic values (Table 2). The largest deviation in the structural determination (0.08 Å) occurred for the Fe−C3 distance in the three-body Fe−N1−C3 pathway. This is again due to the correlation problem of the signal with the two-body contribution from the Cu fragment (Fe−N/C).

Among various fits, it was discovered that there was a correlation between the Cu−O(H) bond length and the Fe−O(H)−Cu bridge angle, indicating that the Cu−O(H) bond distance cannot be determined independently from the angle in the Fe K-edge MS analysis. The two values should thus be viewed in terms of their combined effect, that is, the determination of the longer Fe−Cu distance. The GNXAS fit results showed that the Fe−Cu distance is remarkably consistent, varying within <0.02 Å over all reasonable fits.

(d) Hydroxo Cu K-Edge. The Cu fragment of the hydroxo complex has a distorted square pyramidal coordination with the axial direction defined by a long Cu−O2 bond (2.43 Å) involving a coordinated perchlorate (Figure 1). The rest of the coordination sphere consists of three N2 atoms in the Me_5dien ligand (as compared to four N2 atoms in the oxo complex) and the O atom from the OH^- bridge. The Cu fragment structure is more regular than that of the oxo complex. The average Cu−N2 distance is 2.03 Å with a spread of only 0.02 Å. The Cu−C distances can be grouped into two sets, with an average of 2.82 Å (Cu−C5) with a multiplicity of 6 and an average of 2.97 Å (Cu−C6) with a multiplicity of 3. Therefore, one SS contribution for Cu−N2 and two MS contributions for the three-body Cu−N−C were included in the fit. The three signals have significant magnitudes, as seen from Figure 4. It should be noted that the difference in distances for Cu−C5 and Cu−C6 are around the resolution limit of EXAFS given the range of the available data. Thus, fits with one averaged signal for the nine Cu−N−C configurations were also attempted. These fits, however, gave an *R* value that was more than doubled, indicating a much less satisfactory fit. As at the Fe K-edge, the MS contribution from the Fe−O(H)−Cu bridge configuration is relatively weak, contributing mainly to the FT peak at ∼3.5 Å. Its inclusion in the fit was significant, however, with the *R* value decreasing by 65%.

In addition to the contributions from the bridge and Me_5dien ligands, three more waves were added to the total EXAFS signal. They originate from the interactions of Cu with the counterion $[OClO_3]^-$. The closest oxygen, O2, is directly coordinated to Cu and Cu−O2 is partly responsible for the signal in the FT region at ∼2.1 Å. Without this contribution, this FT area is not at all well fit. The SS pathway Cu−O3 and MS pathway Cu−O2−Cl were introduced to account for part of the FT peak between 2.8 and 3.2 Å (Figure 5d). Some high-frequency components in the EXAFS itself were also better matched as a result of the inclusion of these contributions.

The results in Table 2 indicate that the first-shell distances (Cu−O(H) and Cu−N1) were determined within 0.01 Å of the crystallographic values and the outer shell distances were within 0.03 Å. The angles corresponding to the four three-body signals were determined within 4° with the Cu−O(H)−Fe angle being 161°. The regularity of the Cu fragment is reflected in the small bond variances for the Cu−C5 (0.002 Å^2) and Cu−C6 (0.002 Å^2) distances and the small angle variances for the Cu−N2−C5 (6×10^0 deg^2) and Cu−N2−C6 (3×10^0 deg^2) angles.

One point deserves elaboration. Three of the four three-body interactions included in the fit have an angle less than 150°. Normally, MS effects contribute less significantly for a three-body configuration with an angle <150°. To evaluate whether SS or MS is dominant for these three contributions, SS fits were also attempted including Cu−C5, Cu−C6, and Cu−Cl as two-body signals. The theoretical signal generated by SS fits was in equally good agreement with the experimental data, as indicated by the *R* values. This information, however, was misleading. The structural parameters obtained from the SS fits had a large deviation from the crystallographic values (up to 0.09 Å) for the parameters associated with these signals. An inspection of the individual fitted signals showed that the three-body MS pathway $\gamma^{(3)}$ was out-of-phase and of the same order of magnitude as the two-body contribution $\gamma^{(2)}$, with $\gamma^{(3)}$ being slightly weaker. It is therefore important to include both $\gamma^{(2)}$ and $\gamma^{(3)}$ in the calculation of the signals in question. This MS effect along with the high multiplicity of the pathways for Cu−N2−C5/6 and the small bond variances for these three signals contributes to the relatively strong EXAFS signals. Thus, care needs to be taken when selecting MS signals for inclusion in the fit. Individual $\gamma^{(2)}$ and $\gamma^{(3)}$ should be checked and weighed to determine the dominant feature in the calculation of MS contributions.

EXAFS. Multiple-Edge Fitting. Multiple-edge fitting was performed to generate one set of fitting results that contained information on both photoabsorbers where the parameters for the common pathway was constrained to be the same. The

three-body Fe−X−Cu configuration was introduced as a MS signal with contributions from both Fe and Cu.

(a) Oxo Complex. In addition to the three-body Fe−O−Cu signal, the same set of SS and MS signals used in the single-edge fits were included as separate Fe K-edge and Cu K-edge contributions for the oxo complex, namely five SS signals (Fe−O, Fe−N1, Fe−C1, Cu−O, and Cu−N2) and three MS signals (Fe−N1−C2, Fe−N1−C3, and Cu−N2−C5).

The simultaneous refinement of Fe and Cu data gave results that on average were of the same quality as those from the single-edge fits (see Table 1). This was expected to be the case, since there is only one common pathway (Fe−O−Cu) and it is known to have a very strong contribution to the single-edge fits.

(b) Hydroxo Complex. In the hydroxo case, due to the complexity of the structure, a few of the weak signals were excluded and several off-diagonal covariance matrix elements were set to zero. In this way, the total number of parameters was kept below the limit set by the minimization routine. The final fit therefore included, in addition to the three-body Fe−O(H)−Cu contribution, six SS signals (Fe−O(H), Fe−N1, Fe−C1, Cu−O(H), Cu−N2, and Cu−O2) and five MS signals (Fe−N1−C2, Fe−N1−C3, Cu−N2−C5, Cu−N2−C6, and Cu−O2−Cl).

Overall, the agreement between the fitting results and the crystallographic data was again quite good (Table 2), except for a few distance determinations. These discrepancies likely resulted from the inability to refine all the needed parameters and from the correlation problem, as seen in the Cu−O(H) distance and the bridge angle. In the case of the bridge structure from the Fe viewpoint, the Fe−O(H) and Fe···Cu distances showed an improved agreement with crystallographic values, being determined within 0.01 Å.

The results from multiple-edge fits demonstrated the reliability and accuracy of using this approach on complex inorganic systems of the type studied herein. The excellent agreement of the multiple-edge fits with the experimental data indicated that the new capability in GNXAS is able to fit a relatively large number of parameters and that a minimal residual function R can be reached. This approach is expected to be especially useful where there are multiple common pathways within the same molecule being studied from two (or more) different absorption edges.

Statistical Analysis and Error Determination. A careful evaluation of the statistical (random) errors associated with the bridge unit metrical details as determined by the MS fits described above was performed using the two-dimensional contour plot to examine the correlation of these parameters. This analysis is applied below for the multiple-edge fits because these used both edges to determine the common pathway. Similar results would be found for the individual edge fits.

(a) Oxo complex. The best multiple-edge fit for the oxo complex had an R value of 0.273×10^{-7}, and the fit was performed by varying a total of 40 fitting parameters. Inspection of the EXAFS residual indicated that all major structural signals were explained. The statistical errors were defined by the parameter space of $R \leq R_{min} + C$, where $R_{min} = 0.273 \times 10^{-7}$ and $C = 0.07 \times 10^{-7}$ for 40 degrees of freedom and 95% confidence level in this case. This gave a 39-dimensional ellipsoidal surface in a 40-parameter space. In order to evaluate the statistical errors associated with the three-body bridge structure determinations, two-dimensional contour plots were calculated. These plots were selected among the parameters having the strongest correlation to reflect the highest error.

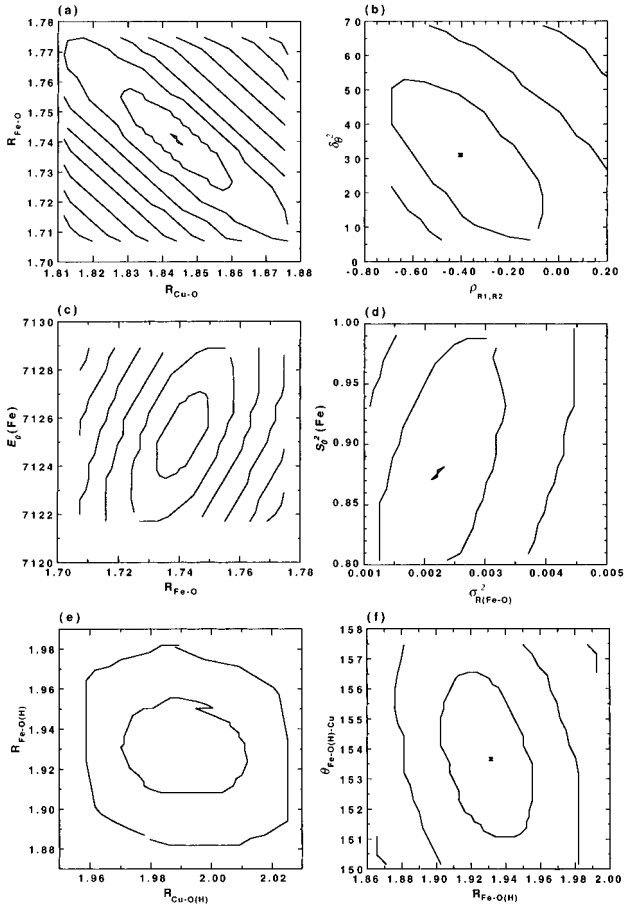

Figure 6. Two-dimensional contour plots for selected parameters in the multiple-edge EXAFS fits which relate to the bridge structure. Oxo: (a) R_{Fe-O} and R_{Cu-O}; (b) angle variance for Fe−O−Cu (δ_θ^2) and the covariance between the Fe−O and Cu−O bonds (ρ_{R_1,R_2}); (c) E_0-(Fe) and R_{Fe-O}; (d) S_0^2(Fe) and Fe−O bond variance ($\sigma^2_{R(Fe-O)}$). Hydroxo: (e) $R_{Fe-O(H)}$ and $R_{Cu-O(H)}$; (f) Fe−O(H)−Cu angle ($\theta_{Fe-O(H)-Cu}$) and $R_{Fe-O(H)}$. The innermost curve corresponds to the 95% confidence interval from which the statistical errors are determined. As discussed in the text, the plots can be used to give the statistical (random) error associated with particular variables.

The correlation between the two bridging bonds Fe−O and Cu−O is shown in Figure 6a. The ellipse shape indicates that there is a well-defined parabolic minimum in the parameter subspace and that the parameters can be determined with high accuracy. From the maximum and minimum values relative to both axes given by the innermost contour (95% level), the statistical errors of the bond lengths were determined to be within ±0.02 Å. These relatively large errors arise because of the high statistical correlation between the two parameters. The plot also shows that the Fe−Cu distance, roughly given by the sum of the Fe−O and Cu−O distances, was 3.58(1) Å. The error was estimated from the range of the sum of the two distances given by any point within the ellipse. This distance is thus determined with a smaller error than for either of the two individual bonds.

To probe the accuracy in the angle determination, the contour plot for the angle variance for Fe−O−Cu (δ_θ^2) and the covariance between the Fe−O and Cu−O bonds (ρ_{R_1,R_2}) was calculated (Figure 6b). The plot shows these two parameters to be correlated and δ_θ^2 to be 30 deg^2. The upper and lower limits of the inner ellipse define $\delta_\theta^2 \approx 10$ and 50 as the 95% confidence limits. Thus, the square roots of the confidence limits, 3.2 and 7.1, respectively, gave the error limits around $\delta_\theta = 5.5°$. As described in ref 23, the standard deviation of the angle from 180° (*i.e.*, $180° - \delta_\theta$) corresponds to the highest

probability of the angle distribution. Thus, while the mean angle is still 180°, the most probable Fe−O−Cu angle was determined to be 174.5 ± 2°. The negative value of ρ_{R_1,R_2}, −0.4(3)°, indicated an anticorrelation between the Fe−O and Cu−O bonds, which is consistent with the vibrational feature of the Fe−O−Cu bridge where a stretch of the Fe−O bond contracts the Cu−O bond (as also seen in Figure 6a). Two more contour plots (Figures 6c and 6d) are presented in the R_{Fe-O}/E_0(Fe) and $\sigma^2_{R(Fe-O)}/S_0^2$(Fe) parameter spaces, showing the importance of correlation with E_0 and S_0^2 in determining the final statistical errors of R and σ^2_R, respectively. The contour plots indicated a strong correlation between these pairs. The errors were determined as following: 7125(2) eV for E_0(Fe), 0.9(1) for S_0^2(Fe), 0.002(1) Å^2 for the Fe−O bond variance $\sigma^2_{R(Fe-O)}$, and 1.74(2) Å for R_{Fe-O}.

(b) Hydroxo Complex. Similar contour plots were calculated for the hydroxo complex. The best fit gave an *R* value of 0.300 × 10^{-8} over the 48 parameters varied. The 95% confidence interval for the statistical errors in the 48-parameter space was defined with the intersection $R \leq R_{min} + C$, where $R_{min} = 0.300 \times 10^{-8}$ and $C = 0.07 \times 10^{-8}$.

Judging from the degree of tilt of the contour plot in Figure 6e, there is virtually no correlation between $R_{Fe-O(H)}$ and $R_{Cu-O(H)}$, which contrasts the strong correlation of the pair in the oxo case. The statistical errors associated with these two bond distances are 1.93(2) and 1.99(2) Å for Fe−O(H) and Cu−O(H), respectively, and the long Fe−Cu distance was found to be 3.81(2) Å. Both $R_{Fe-O(H)}$ (Figure 6f) and $R_{Cu-O(H)}$ (not shown) show anticorrelations with the $\theta_{Fe-O(H)-Cu}$ of about the same magnitude. The correlation between $R_{Cu-O(H)}$ and $\theta_{Fe-O(H)-Cu}$ was evident in the determination of the Fe−O(H)−Cu geometry (as discussed in the results section). Both contour plots showed that the angle was 154° with statistical error of ±3°. Different from what was expected, $\sigma^2_{R(Fe-O)}$ and S_0^2(Fe) were uncorrelated, whereas the contour plots involving E_0(Fe) and $R_{Fe-O(H)}$ gave a similar type of correlation between the pairs as that for the oxo case (not shown).

Angle Dependence of MS Effects. Results from the fits described above can be compared to better understand and illustrate the determining factors in the EXAFS of the Fe−O/O(H)−Cu bridge. It is very clear, both from observations in the FTs and as quantitated by the GNXAS fitting results, that the major structural difference in the two complexes having a significant impact on the EXAFS spectra is the bridge structure. This derives from the significant enhancement in amplitude for the collinear structure[34] due to the forward scattering along the linear path (the "intervening atom effect").

The use of the bridge unit MS effects to accurately determine the structure also depends on successful modeling of the other MS pathways in the molecular fragments (especially the porphyrin from the Fe viewpoint). The fit results show that this is indeed possible with the GNXAS analysis. Thus, while the relative strengths of the three-body MS contributions from the porphyrin were about the same in both the oxo and hydroxo cases (Fe−N1−C2 and Fe−N1−C3), the Fe−O−Cu signal weakened as the angle changed from 178 to 157°, going from the largest contribution among the three MS signals in the oxo to the weakest in the hydroxo complex (Figures 3 and 4). The same amplitude enhancement of the backscattering as in the oxo case was also seen for the Cu data. The fits also showed a somewhat larger bond variance for the Fe−Cu pathway of the three-body signal (compare Tables 1 and 2), suggesting a decreased rigidity of the bridge. This larger bond variance also further weakened the signal in the hydroxo case. The large overall difference in the strength of the signal resulted in the striking change in the region of the FT spectra where the three-body Fe−O/O(H)−Cu signal contributes.

As described above, for the oxo complex a good fit could be obtained only when the Fe−O−Cu MS contribution was included. The strong Fe−O−Cu signal thus enabled an accurate determination of metrical details of the bridge structure. The calculated distance for Fe−Cu from various fits (including multiple-edge fits) was consistently within 0.01 Å of the crystallographic distance of 3.57 Å, and the Fe−O−Cu angle deviated less than 2° from the crystal structure. The relatively weak Fe−O(H)−Cu contribution in the hydroxo complex, on the other hand, made the determination of the structural parameters less accurate. The calculated Fe−Cu distance fluctuated from fit to fit with a deviation between 0.01 and 0.03 Å from the crystallographic value of 3.80 Å, and the average Fe−O(H)−Cu angle was determined to be 153°, deviating by 4° from the crystallographic value. The inclusion of the Fe−O(H)−Cu contribution in fits to the hydroxo data was, however, significant (with the *R* value decreasing by ∼25 and ∼65% as discussed above). The angle determination of the Fe−O/O(H)−Cu signal of the two complexes is thus quite accurate, and the results obtained from both the Fe and Cu K-edge data are consistent. The angular sensitivity of MS effects was confirmed by a theoretical calculation of the Fe−O−Cu signal as a function of angle, as was done in the angle determination of a series of iron nitrosyl complexes.[24] The results (not shown) followed a systematic decrease in magnitude of the signal as the angle varied from 180 to 90°, with the significant amplitude enhancement occurring above 150°.

Conclusions and Summary

The results of this study demonstrate the successful delineation of MS contributions from a rigid porphyrin and a linear or nonlinear bridge structure containing a Fe−X−Cu bridge. From GNXAS analysis, accurate metrical determination (distances and angles) were obtained. The complexes studied offered an opportunity to perform the analysis at two different edges (Fe and Cu). A new feature of GNXAS enabled combining information from both edges through multiple-edge fits where parameters for a common structural fragment (the bridge path) were constrained to be the same.

As discussed above, the distances and angles for the bridge in both the oxo and hydroxo cases were accurately determined by the MS EXAFS analysis. In general, the errors in EXAFS determinations are dominated by systematic errors (from data collection and intrinsic limitations in the theory) and correlation effects.[34] The contour plot calculations provided a very useful approach in establishing upper limits on the random errors for the determined parameters where correlation contributed significantly. A more global estimate of error (systematic and random) comes from comparison of the difference of the EXAFS and crystallographically determined structures. The average deviation from crystal structure values for all distances determined in the final single- and multiple-edge fits is 0.018 Å. If the two longer light atom distances (>4 Å) which have quite low magnitude are excluded, then the difference is 0.014 Å. The average angle deviation is 1.5°. This EXAFS analysis of complexes whose structures are known with high accuracy is an important step toward the application of this approach to unknown systems, in particular binuclear bridged sites in metalloenzymes.

This work contributes to the general problem of the structural definition of linear and nonlinear homo- and heterometallic M−X−M′ bridges that may occur in synthetic and biological bridged assemblies. Biological assemblies, in which two

discrete fragments are juxtaposed wholly or in part by one or more covalent bridges, have been noted elsewhere.[44] Of these, *hetero*metallic bridges established by X-ray diffraction are found in superoxide dismutase (Cu^{II}−(imidazolate)−Zn^{II})[45] and purple acid phosphatase (Fe^{III}−(RCO_2)(OH)−Zn^{II}).[46] The putative Fe−X−Ni bridge in carbon monoxide dehydrogenase remains undefined.[47,48] The largest number of real and potential heterometal bridges within one type of metalloprotein is, however, found with the binuclear sites of heme−copper oxidases. As noted at the outset, the two oxidase crystal structures recently reported[9,10] do not exhibit the discrete bridges anticipated on the basis of exchange coupling between Fe(III) and Cu(II) in the oxidized enzymes. Perhaps one or both metal centers became reduced over the course of X-ray crystallographic data collection, or perhaps the microscopic pH around the binuclear center was such as to violate the Fe−O(H)−Cu bridge considered probable for the quinol oxidase from *Bacillus subtilis* by Fann *et al.*[28], on the basis of ENDOR and Fe and Cu EXAFS. Results for this enzyme are not in accord with the analysis by Powers *et al.*[27] favoring a S/Cl bridging atom. The Fe···Cu separation is reported as 3.7 Å. Apparent Fe···Cu separations of 3.89 Å (Cu) and 4.04 Å (Fe) have been determined for the oxidized beef heart enzyme by EXAFS analysis of the indicated absorber.[29] Neither of these is close to the present crystallographic value (4.5 Å),[10] the shorter distance being nearer the crystallographic result for the hydroxo complex (3.80 Å).[13] An S/Cl bridging atom is reported for the beef heart enzyme.[29] Significantly, no EXAFS spectrum of a heme−copper oxidase yet displays the intervening atom effect consistent with a linear Fe−O−Cu bridge.

In addition to the resting form(s) of the oxidases, enzymes inhibited by exogenous anions such as fluoride, cyanide, formate, and azide may be profitably interrogated by XAS. Inhibition presumably arises by anion binding to one or both metal centers in the binuclear site,[49] as we have argued on the basis of certain spectroscopic properties of structurally characterized Fe^{III}−CN−Cu^{II} bridged complexes.[14−16] The continued availability of structurally defined heme−copper synthetic bridged assemblies and application of the GNXAS methodology to their EXAFS spectra could afford further clarification of the nature of the binuclear site in the oxidized and inhibited forms of the enzymes. Work directed toward these ends is currently in progress in our laboratories.

Acknowledgment. This research was supported by NSF CHE 94-23181 and NIH RR-01209 (to K.O.H.) and by NSF CHE 92-08387 and 95-23830 (to R.H.H.). We are grateful to Tami E. Westre for helpful discussions about the XAS edge spectra. The Stanford Synchrotron Radiation Laboratory is supported by the Department of Energy, Office of Basic Energy Sciences, Divisions of Chemical and Materials Sciences, and in part by the National Institutes of Health, National Center for Research Resources, Biomedical Research Technology Program and by the DOE Office of Health and Environmental Research.

IC960021N

(44) Holm, R. H. *Pure Appl. Chem.* **1995**, *67*, 217.
(45) Bovine erythrocyte enzyme: (a) Tainer, J. A.; Getzoff, E. D.; Beem, K. M.; Richardson, J. S.; Richardson, D. C. *J. Mol. Biol.* **1982**, *160*, 181. (b) Tainer, J. A.; Getzoff, E. D.; Richardson, J. S.; Richardson, D. C. *Nature* **1983**, *306*, 284.
(46) Kidney bean enzyme: Sträter, N.; Klabunde, K.; Tucker, P.; Witzel, H.; Kerbs, B. *Science* **1995,** *268*, 1489.
(47) Qui, D.; Kumar, M.; Ragsdale, S. W.; Spiro, T. G. *Science* **1994**, *264*, 817.
(48) Xia, J.; Dong, J.; Wang, S.; Scott, R. A.; Lindahl, P. A. *J. Am. Chem. Soc.* **1995**, *117*, 7065.
(49) This point has been raised frequently in the heme−copper oxidase literature. See, for example: (a) Palmer, G. *J. Bioenerg. Biomembr.* **1993**, *25*, 145. (b) Baker, G. M.; Gullo, S. M. *Biochemistry* **1994**, *33*, 8058.